# Reduction Methodology for Fluctuation Driven Population Dynamics

Denis S. Goldobin[1,2] Matteo di Volo,[3] and Alessandro Torcini[3,4,5,*]

[1]*Institute of Continuous Media Mechanics, Ural Branch of RAS, Acad. Korolev Street 1, 614013 Perm, Russia*
[2]*Department of Theoretical Physics, Perm State University, Bukirev Street 15, 614990 Perm, Russia*
[3]*Laboratoire de Physique Théorique et Modélisation, Université de Cergy-Pontoise, CNRS,*
*UMR 8089, 95302 Cergy-Pontoise cedex, France*
[4]*CNR—Consiglio Nazionale delle Ricerche—Istituto dei Sistemi Complessi, via Madonna del Piano 10, I-50019 Sesto Fiorentino, Italy*
[5]*INFN Sezione di Firenze, Via Sansone 1, I-50019 Sesto Fiorentino, Florence, Italy*

Lorentzian distributions have been largely employed in statistical mechanics to obtain exact results for heterogeneous systems. Analytic continuation of these results is impossible even for slightly deformed Lorentzian distributions due to the divergence of all the moments (cumulants). We have solved this problem by introducing a "pseudocumulants" expansion. This allows us to develop a reduction methodology for heterogeneous spiking neural networks subject to extrinsic and endogenous fluctuations, thus obtaining a unified mean-field formulation encompassing quenched and dynamical sources of disorder.

*Introduction.*—The Lorentzian distribution (LD) is the second most important stable distribution for statistical physics (after the Gaussian) [1]. It is expressible in a simple analytic form: $L(y) = \{[\pi^{-1}\Delta]/[\Delta^2 + (y - y_0)^2]\}$, where $y_0$ is the peak location and $\Delta$ is the half-width at half-maximum (HWHM). In particular, for a system with random heterogeneities distributed according to an LD, the average observables can be estimated exactly via the residue theorem [2].

This approach has found a wide application in physics: from quantum optics, where it was first employed to account exactly for the presence of heterogeneities in laser emissions [2,3], to condensed matter, where it was possible to obtain exact results for the Anderson localization in three dimensions [4] by assuming an LD for the potential disorder within the Lloyd model [5]. Furthermore, a Lorentzian formulation makes it possible to obtain exact results for the collective dynamics of heterogeneous oscillators in various contexts [6,7]. Moreover, LDs emerge naturally for the phases of self-sustained oscillators driven by common noise [8,9].

More recently, the Ott-Antonsen (OA) ansatz [10,11] yielded closed mean-field (MF) equations for the dynamics of the synchronization order parameter for globally coupled phase oscillators on the basis of a wrapped LD of their phases. The nature of these phase elements can vary from biological and chemical oscillators [12,13] to superconducting Josephson junctions [14,15] and directional elements like active rotators [16,17] or magnetic moments [18].

A very important recent achievement has been the application of the OA ansatz to heterogeneous globally coupled networks of spiking neurons—specifically, of quadratic integrate-and-fire (QIF) neurons [19,20]. In particular, this formulation makes it possible to derive a closed low-dimensional set of macroscopic equations describing exactly the evolution of the population firing rate and of the mean membrane potential [21]. In the very last years the Montbrió-Pazó-Roxin (MPR) model [21] is emerging as a representative of a new generation of neural mass models able to successfully reproduce relevant features of neural dynamics [22–33].

However, the OA ansatz (as the MPR model) is unable to capture the role of random fluctuations naturally present in real systems. In brain circuits, the neurons are sparsely connected and *in vivo* the presence of noise is unavoidable [34]. These different sources of fluctuations are at the origin of fundamental aspects of neural dynamics such as the balance among excitation and inhibition [35,36] and the emergence of collective behaviors [37]. The inclusion of these ingredients in MF models has been so far limited to homogeneous neural populations [38–43]. The main scope of this Letter is to fill such a gap by developing a unified MF formalism for heterogeneous noisy neural networks encompassing quenched and dynamical disorders.

Furthermore, in this Letter we introduce a general reduction methodology for dealing with deviations from the LD on the real axis. This approach is based on the expansion of the characteristic function in terms of "pseudocumulants," thus avoiding the divergences related to the expansion in conventional moments or cumulants. The implementation and benefits of this formulation are demonstrated for heterogeneous populations of QIF neurons in the presence of extrinsic and endogenous noise sources, where the conditions for an LD of the membrane potentials [21] are violated as in [44,45]. In particular, we

will derive a hierarchy of low-dimensional MF models for noisy globally coupled populations and deterministic sparse random networks, with a particular emphasis on the emergence of fluctuation driven collective oscillations (COs). For all these realistic setups, we will show that our formulation reproduces quantitatively the network dynamics, while the MPR model fails to give even a qualitative picture.

*Heterogeneous populations of QIF neurons.*—Let us consider a globally coupled network of $N$ heterogeneous QIF neurons, whose membrane potentials $\{V_j\}$, with $j = 1, \ldots, N$, evolve as

$$\dot{V}_j = V_j^2 + I_j, \qquad I_j = I_0 + \eta_j + J_j s(t) + \sigma_j \xi_j(t), \quad (1)$$

where $I_0$ is the external dc current, $\eta_j$ the neural excitability, and $J_j s(t)$ the recurrent input due to the neural activity $s(t)$ mediated by the synaptic coupling $J_j$. Furthermore, each neuron is subject to an additive Gaussian noise of amplitude $\sigma_j = \sigma(\eta_j, J_j)$, where $\langle \xi_j(t)\xi_l(t')\rangle = 2\delta_{jl}\delta(t - t')$ and $\langle \xi_j \rangle = 0$. The $j$th neuron emits a spike whenever the membrane potential $V_j$ reaches $+\infty$, and it is immediately reset at $-\infty$ [46]. For instantaneous synapses, in the limit $N \to \infty$, the activity of the network $s(t)$ will coincide with the population firing rate $r(t)$ [21]. Furthermore, we assume that the parameters $\eta_j$ ($J_j$) are distributed according to an LD $g(\eta)$ [$h(J)$] with median $\eta_0$ ($J_0$) and HWHM $\Delta_\eta$ ($\Delta_J$).

In the thermodynamic limit, the population dynamics can be characterized in terms of the probability density function (PDF) $w(V, t|\mathbf{x})$ with $\mathbf{x} = (\eta, J)$, which obeys the following Fokker-Planck equation (FPE):

$$\partial_t w(V, t|\mathbf{x}) + \partial_V[(V^2 + I_\mathbf{x})w(V, t|\mathbf{x})] = \sigma_\mathbf{x}^2 \partial_V^2 w(V, t|\mathbf{x}), \quad (2)$$

where $I_\mathbf{x} \equiv I_0 + \eta + Jr(t)$. In [21], the authors made the ansatz such that, for any initial PDF $w(V, 0|\mathbf{x})$, the solution of Eq. (2) in the absence of noise converges to an LD $w(V, t|\mathbf{x}) = a_\mathbf{x}/\{\pi[a_\mathbf{x}^2 + (V - v_\mathbf{x})^2]\}$, where $v_\mathbf{x}$ is the mean membrane potential and $r_\mathbf{x}(t) = \lim_{V\to\infty} V^2 w(V, t|\mathbf{x}) = (a_\mathbf{x}/\pi)$ the firing rate for the $\mathbf{x}$ subpopulation. This Lorentzian ansatz has been shown to correspond to the OA ansatz for phase oscillators [21] and, joined with the assumption that the parameters $\eta$ and $J$ are independent and Lorentzian distributed, leads to the derivation of exact low-dimensional macroscopic evolution equations for globally coupled deterministic QIF networks.

*Characteristic function and pseudocumulants.*—In order to extend the MPR approach [21] to noisy systems, we introduce the characteristic function for $V_\mathbf{x}$, i.e., the Fourier transform of its PDF, namely

$$\mathcal{F}_\mathbf{x}(k) = \langle e^{ikV_\mathbf{x}} \rangle = \text{p.v.} \int_{-\infty}^{+\infty} e^{ikV_\mathbf{x}} w(V_\mathbf{x}, t|\mathbf{x})dV_\mathbf{x}.$$

In this framework, the FPE [Eq. (2)] can be rewritten as

$$\partial_t \mathcal{F}_\mathbf{x} = ik[I_\mathbf{x}\mathcal{F}_\mathbf{x} - \partial_k^2 \mathcal{F}_\mathbf{x}] - \sigma_\mathbf{x}^2 k^2 \mathcal{F}_\mathbf{x}. \quad (3)$$

For more details, see [47]. Under the assumption that $\mathcal{F}_\mathbf{x}(k, t)$ is an analytic function of the parameters $\mathbf{x}$, one can estimate the average characteristic function for the population $F(k, t) = \int d\eta \int dJ \mathcal{F}_\mathbf{x}(k, t)g(\eta)h(J)$ and the corresponding FPE via the residue theorem, with the caution that different contours have to be chosen for positive (upper half-plane) and negative (lower half-plane) $k$. Hence, the FPE is given by

$$\partial_t F = ik[H_0 F - \partial_k^2 F] - |k|D_0 F - S_0^2 k^2 F, \quad (4)$$

where $H_0 = I_0 + \eta_0 + J_0 r$, $D_0 = \Delta_\eta + \Delta_J r$, and $S_0^2 = \sigma_{[\eta_0 + i\Delta_\eta \text{sign}(k), J_0 + i\Delta_J \text{sign}(k)]}^2 = \mathcal{N}_R + i\mathcal{N}_I$. For the logarithm of the characteristic function $F(k) = e^{\Phi(k)}$, one obtains the following evolution equation:

$$\partial_t \Phi = ik[H_0 - \partial_k^2 \Phi - (\partial_k \Phi)^2] - |k|D_0 - S_0^2 k^2. \quad (5)$$

In this context, the Lorentzian ansatz amounts to set $\Phi_L = ikv - a|k|$ [51]. By substituting $\Phi_L$ in Eq. (5) for $S_0 = 0$, one gets

$$\dot{v} = H_0 + v^2 - a^2, \qquad \dot{a} = 2av + D_0, \quad (6)$$

which coincides with the two dimensional MF model found in [21] with $r = a/\pi$.

In order to consider deviations from the LD, we analyze the following general polynomial form for $\Phi$:

$$\Phi = -a|k| + ikv - \sum_{n=2}^{\infty} \frac{q_n|k|^n + ip_n|k|^{n-1}k}{n}. \quad (7)$$

The terms entering in the above expression are dictated by the symmetry of the characteristic function $\mathcal{F}_\mathbf{x}(k)$ for real-valued $V_\mathbf{x}$, which is invariant for a change of sign of $k$ joined to the complex conjugation. For this characteristic function, neither moments nor cumulants can be determined [48]. Therefore, we will introduce the notion of "pseudocumulants," defined as follows:

$$W_1 \equiv a - iv, \qquad W_n \equiv q_n + ip_n. \quad (8)$$

By inserting the expansion [Eq. (7)] in Eq. (5), one gets the evolution equations for the pseudocumulants, namely

$$\dot{W}_m = (D_0 - iH_0)\delta_{1m} + 2(\mathcal{N}_R + i\mathcal{N}_I)\delta_{2m}$$
$$+ im\left(-mW_{m+1} + \sum_{n=1}^{m} W_n W_{m+1-n}\right), \quad (9)$$

where for simplicity we assumed $k > 0$. It can be shown [47] that the modulus of the pseudocumulants scales as

$|W_m| \propto |S_0|^{2(m-1)}$ with the noise amplitude; therefore, it is justified to consider an expansion limited to the first two pseudocumulants. In this case, one obtains the following MF equations:

$$\dot{r} = (\Delta_\eta + \Delta_J r + p_2)/\pi + 2rv, \qquad (10a)$$

$$\dot{v} = I_0 + \eta_0 + J_0 r - \pi^2 r^2 + v^2 + q_2, \qquad (10b)$$

$$\dot{q}_2 = 2\mathcal{N}_R + 4(p_3 + q_2 v - \pi p_2 r), \qquad (10c)$$

$$\dot{p}_2 = 2\mathcal{N}_I + 4(-q_3 + \pi q_2 r + p_2 v). \qquad (10d)$$

As we will show in the following, this four dimensional model (with the simple closure $q_3 = p_3 = 0$) is able to accurately reproduce the macroscopic dynamics of noisy globally coupled and deterministic sparse QIF networks. Therefore, the MF model [Eq. (10)] represents an extension of the MPR model to systems subject to extrinsic and/or endogenous noise sources.

As shown in [47], the definitions of $r = \lim_{V \to \infty} V^2 w(V, t)$ and $v = \text{p.v.} \int_{-\infty}^{+\infty} V w(V, t) dV$ in terms of $w(V, t)$ reported in [21] for the LD are not modified by considering corrective terms $\{q_n, p_n\}$ of any order. Furthermore, $q_2$ ($p_2$) can be interpreted as an analog of *kurtosis* (*skewness*) for a distorted Gaussian distribution [47].

*Globally coupled network with extrinsic noise.*—To show the quality of the MF formulation [Eq. (10)], let us consider a globally coupled network of QIF neurons, each subject to an independent additive Gaussian noise term of amplitude $\sigma$ (i.e., $\mathcal{N}_R = \sigma^2$, $\mathcal{N}_I = 0$). In this setup, the model [Eq. (10)] is able to reproduce the macroscopic dynamics of the network in different dynamical regimes relevant for neural systems.

Let us first consider the asynchronous dynamics, which corresponds to a fixed point solution $(\bar{r}, \bar{v}, \bar{q}_2, \bar{p}_2)$ for Eq. (10). As shown in Figs. 1(a) and 1(b), in the asynchronous state (AS), the MF model [Eq. (10)] reproduces quite well the population firing rate and the mean membrane potential obtained by the network simulations, while the deviations from the MPR model (dashed magenta lines) become appreciable for noise amplitudes $\tilde{\sigma} \equiv (\sigma/\sigma_*) \sim \mathcal{O}(1)$, where $\sigma_*$ represents a reference noise scale defined in [47]. Furthermore, the corrections $q_2$ and $p_2$ scale as $\propto \tilde{\sigma}^2$ as expected [see Figs. 1(c) and 1(d)]. The truncation to the second order of the expansion [Eq. (9)], which leads to Eq. (10), is largely justified in the whole range of noise amplitude here considered. Indeed, as displayed in Fig. 1(e), $|W_1| \sim \mathcal{O}(10^{-2})$ and $|W_2| \sim \mathcal{O}(10^{-4})$, while the moduli of the other pseudocumulants are definitely smaller (for more details, see [47]).

For lower levels of heterogeneity, one can observe the emergence of noise induced COs. The analysis of the bifurcation diagram of the MF model [Eq. (10)] in the plane $(\tilde{\sigma}, \Delta_J)$ reveals the existence of three dynamical states:
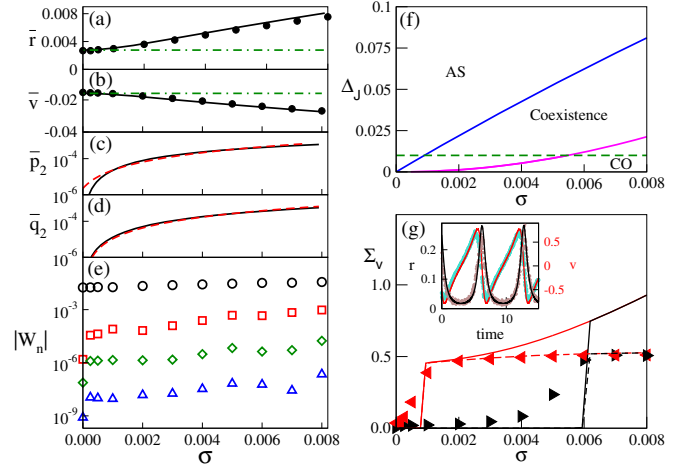


FIG. 1. (a)–(e) Asynchronous Dynamics. Stationary values $\bar{r}$ (a), $\bar{v}$ (b), $\bar{p}_2$ (c), $\bar{q}_2$ (d), and $|W_n|$ (e) versus the rescaled noise amplitude $\tilde{\sigma} = \sigma/\sigma_*$ [47]. (a),(b) Symbols refer to network simulations with $N = 16\,000$, solid line to the MF model [Eq. (10)], dashed-dotted (green) lines are the values of $\bar{r}$ and $\bar{v}$ for the MPR model. In (c),(d), the dashed red lines refer to a quadratic fit to the data. In (e), the symbols from top to bottom denote $|W_1|$, $|W_2|$, $|W_3|$, and $|W_4|$. Other parameters: $I_0 = 0.000\,1$, $J_0 = -0.1$, $\Delta_J = 0.1$, $\sigma_* = 0.004\,58$. (f),(g) Emergence of COs. (f) Bifurcation diagram in the plane $(\tilde{\sigma}, \Delta_J)$: the magenta (blue) solid line denotes subcritical Hopf bifurcations from the AS to COs (saddle-node bifurcations of limit cycles). The horizontal green dashed line corresponds to the case studied in (g). (g) Standard deviations $\Sigma_v$ obtained for quasiadiabatic variation of $\tilde{\sigma}$. Lines (symbols) refer to MF (network) simulations: black (red) lines and right (left) triangles are obtained by increasing (decreasing) $\sigma$. Solid (dashed) lines refer to the pseudocumulant reduction [Eq. (9)] arrested to the second (third) order. In the inset are reported $r$ and $v$ versus time for $\sigma = 0.143$: dots refer to network simulations with $N = 32000$ and lines to MF results. Other parameters: $I_0 = 0.38$, $J_0 = -6.3$, $\Delta_J = 0.01$, $\sigma_* = 0.014$, $\eta_0 = \Delta_\eta = 0$. Bifurcation lines in (f) have been obtained by employing the software XPP AUTO [52].

asynchronous, oscillatory, and a regime of coexistence of the AS and COs. In particular, a large heterogeneity $\Delta_J$ prevents the occurrence of COs, which are instead promoted by strong noise. As shown in Fig. 1(f), the regimes are delimited by bifurcation lines, that is, COs emerge via subcritical Hopf bifurcations from the AS (black solid line) and disappear via a saddle-node bifurcation of limit cycles (red solid line). The dynamical regimes induced by noise cannot be captured by the MPR model, which would predict only the AS corresponding to $\tilde{\sigma} = 0$.

Let us focus on a specific cut in the plane $(\tilde{\sigma}, \Delta_J)$; namely, we fix $\Delta_J = 0.01$ [green dashed line in Fig. 1(f)]. In this case, the MF reveals that the AS loses stability in favor of noise driven COs at $\tilde{\sigma}_{HB} \simeq 0.393$ due to a subcritical Hopf bifurcation and that COs can survive down to $\tilde{\sigma}_{SN} \simeq 0.068$, where they disappear via a saddle-node bifurcation. These transitions can be characterized in terms of the standard deviation $\Sigma_v$ of the mean membrane

potential, which is zero (finite) in the AS (CO regime) in the thermodynamic limit. We report in Fig. 1(g) $\Sigma_v$ versus $\tilde{\sigma}$ as obtained from adiabatic simulations of the MF (solid and dashed lines) and of the network with $N = 64\,000$ (triangles). Apart from the finite time and size effects that prevent the vanishing of $\Sigma_v$ in the AS, the network simulations reveal the same dynamical behaviors as the MF. Furthermore, as shown in the inset of panel (g), the model [Eq. (10)] is able to accurately reproduce the time evolution of $v$ and $r$ also during COs for moderate noise amplitudes (namely, $\tilde{\sigma} = 0.143$). However, at larger noise amplitudes, in order to obtain a good quantitative agreement between MF and network simulations, one should extend the pseudocumulant reduction [Eq. (9)] to the third order [dashed lines in panel (g)].

*Sparse networks exhibiting endogenous fluctuations.*— Let us now consider a sparse network characterized by randomly distributed in degrees $k_j$. As shown in [44,53], the quenched disorder in the synaptic inputs can be rephrased in terms of heterogeneous synaptic couplings. In particular, by assuming an LD for the $k_j$ with median $K$ and HWHM $\Delta_k = \Delta_0 K$, we can hypothesize for the MF formulation that the neurons are fully coupled but with Lorentzian distributed couplings $J_j = (J_0 k_j / K)$ with median $J_0$ and HWHM $\Delta_J = |J_0| \Delta_0$. Furthermore, to evaluate the fluctuations in the synaptic inputs, we can assume at an MF level that each neuron $j$ receives $k_j$ Poissonian spike trains characterized by a rate $r$ [38]. This amounts to having an average synaptic input $J_j r(t)$ with Gaussian fluctuations of variance $\sigma_j^2 = [J_0^2 k_j r(t) / 2K^2]$. Therefore, each neuron $j$ will be subject to a noise of intensity $\sigma_j^2 = (|J_0 J_j|/2K) r(t)$; thus, $\mathcal{N}_R = (J_0^2 r / 2K)$ and $\mathcal{N}_I = -(J_0^2 \Delta_0 r / 2K) = -\Delta_0 \mathcal{N}_R$.

For this random network, we report in Fig. 2(a) a bifurcation diagram in the plane $(|J_0|, I_0)$ estimated for the MF model [Eq. (10)]. We find the same three dynamical regimes observed in the globally coupled case but differently arranged and separated by different bifurcation lines. In particular, the AS emerges for sufficiently large excitatory drive $I_0$, where most neurons are suprathreshold and the dynamics is essentially mean driven [54]. The coupling strength $|J_0|$ controls the amplitude of current fluctuations; indeed, for increasing $|J_0|$ fluctuation, driven COs emerge via supercritical Hopf bifurcations (black solid line). For even larger coupling beyond a subcritical Hopf bifurcation (red solid line), a coexistence among the AS and CO can be observed. However, the nature of this AS is different from that at low $|J_0|$: this is a fluctuation driven regime, where excitatory drive and recurrent inhibition tend to balance [35,36].

As shown in Figs. 2(b) and 2(c), network simulations are in good agreement with the MF predictions for low and high dc currents, which can be appreciated by comparing the standard deviations $\Sigma_v$ obtained for networks of
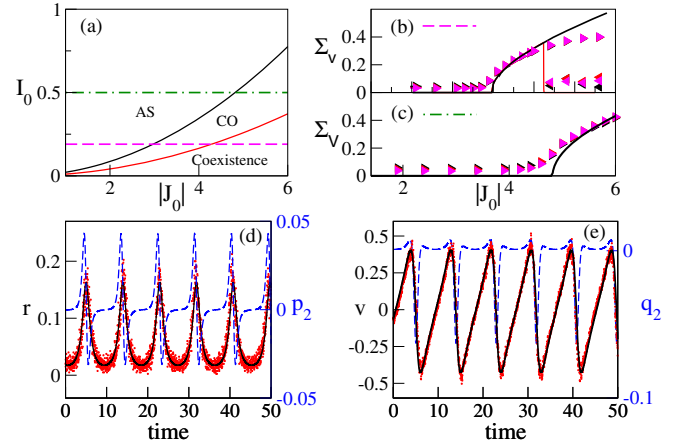


FIG. 2. Sparse Networks. (a) Bifurcation diagram in the plane $(|J_0|, I_0)$: the black (red) line denotes supercritical (subcritical) Hopf bifurcations from the AS to COs. The magenta dashed (green dot-dashed) line indicates the case examined in panel (b) for $I_0 = 0.19$ [panel (c) for $I_0 = 0.50$]. (b),(c) $\Sigma_v$ obtained for quasiadiabatic variation of $|J_0|$. Solid line (colored symbols) refers to MF (network) results: black (red) lines and right (left) triangles are obtained by increasing (decreasing) $|J_0|$. The symbol colors denote different network sizes: namely, $N = 10\,000$ (black), 15 000 (red), and 20 000 (magenta). The values are averaged over eight random realizations of the network. For $J_0 = -3.7$ and $I_0 = 0.19$, the MF evolution of $r$ ($p_2$) and $v$ ($q_2$) is displayed in (d) and (e) as black solid (blue dashed) lines, respectively. In (d),(e), the symbols refer to network simulations with $N = 40\,000$. In all panels, the parameters are $K = 4000$, $\Delta_0 = 0.01$, $\eta_0 = \Delta_\eta = 0$.

different sizes with the findings of the model [Eq. (10)]. Furthermore, at intermediate coupling, the oscillations of $r$ and $v$ in the network are very well captured by the MF dynamics [see Figs. 2(d) and (e)]. However, as shown in panel (b) for $I_0 = 0.19$, the amplitudes of the COs are slightly overestimated by the MF at sufficiently large $|J_0| > 4.5$. No discrepancies are observable in panel (c) for the same range of $|J_0|$. As shown in [47], this is due to the fact that the rescaled noise amplitudes are definitely smaller in this latter case.

As shown in [44], the MPR model, even with the inclusion of the quenched disorder due to the heterogeneous in degrees, is unable to predict the oscillatory and coexistence regimes displayed by the sparse inhibitory network. Therefore, it is fundamental to take in account corrections to the Lorentzian ansatz due to endogenous fluctuations. Indeed, as shown in Figs. 2(d) and (e), the evolution of $r$ and $v$ is clearly guided by that of the corrective terms $p_2$ and $q_2$ displaying regular oscillations.

*Conclusions.*—A fundamental aspect that renders the LD difficult to employ in a perturbative approach is that all moments and cumulants diverge. However, to cure this aspect, one can introduce an expansion in "pseudocumulants" of the characteristic function. As we have shown, this expansion can be fruitfully applied to build in full

generality a hierarchy of low-dimensional neural mass models able to reproduce, with the desired accuracy, firing rate and mean membrane potential evolutions for heterogeneous spiking neural networks in the presence of extrinsic and intrinsic fluctuations.

One key feature of the MPR formulation, as of our reduction methodology, is the ability of these MF models to capture transient synchronization properties and oscillatory dynamics present in the spiking networks [22,26,27,32] but that are lost in usual rate models, e.g., Wilson-Cowan [55]. However, our MF formulation can encompass further fundamental aspects of brain circuits beyond heterogeneity as sparseness in the synaptic connections and background noise [34] not envisioned in the MPR model. Therefore, our mass model is able to reproduce spiking network dynamics induced by various noise sources, which cannot be predicted within the MPR framework developed for globally coupled deterministic populations.

MF formulations for heterogeneous networks subject to extrinsic noise have been examined in the context of the *circular cumulants* expansion [43,45,56,57]. However, any finite truncation of this expansion leads to a divergence of the population firing rate [57]. Our formulation does not suffer from these strong limitations and even the definitions of the macroscopic observables are not modified by considering higher order corrective terms [47].

In order to clarify the limits of applicability of our formulation, we have introduced in [47] a reference noise scale up to which a good quantitative agreement between network simulations and the MF model [Eq. (10)] should be expected. Furthermore, preliminary results suggest that our approach can be extended also to noisy homogeneous networks displaying sustained firing activities [47].

Potentially, the introduced framework can be fruitfully applied to generalize previous results obtained for many body systems with LD heterogeneities [2,5,58].

[*]Corresponding author.
alessandro.torcini@cyu.fr

[1] V. M. Zolotarev, *One-Dimensional Stable Distributions, Translations of Mathematical Monographs* (American Mathematical Society, Providence, 1986), Vol. 65.
[2] E. Yakubovich, Sov. Phys. JETP **28**, 160 (1969).
[3] W. E. Lamb, Jr., Phys. Rev. **134**, A1429 (1964).
[4] P. W. Anderson, Phys. Rev. **109**, 1492 (1958).
[5] P. Lloyd, J. Phys. C **2**, 1717 (1969).
[6] M. I. Rabinovich and D. I. Trubetskov, Oscillations and Waves: In Linear and Nonlinear Systems (Springer Netherlands, Dordrecht, 1989), Vol. **50**.
[7] J. D. Crawford, J. Stat. Phys. **74**, 1047 (1994).
[8] D. S. Goldobin and A. Pikovsky, Phys. Rev. E **71**, 045201 (R) (2005).
[9] D. S. Goldobin and A. V. Dolmatova, Commun. Nonlinear Sci. Numer. Simul. **75**, 94 (2019).
[10] E. Ott and T. M. Antonsen, Chaos **18**, 037113 (2008).
[11] E. Ott and T. M. Antonsen, Chaos **19**, 023117 (2009).
[12] A. T. Winfree, J. Theor. Biol. **16**, 15 (1967).
[13] Y. Kuramoto, *Chemical Oscillations, Waves, and Turbulence* (Dover Publication, Mineola, 2003).
[14] S. Watanabe and S. H. Strogatz, Physica (Amsterdam) **74D**, 197 (1994).
[15] S. A. Marvel and S. H. Strogatz, Chaos **19**, 013132 (2009).
[16] A. V. Dolmatova, D. S. Goldobin, and A. Pikovsky, Phys. Rev. E **96**, 062204 (2017).
[17] V. Klinshov and I. Franović, Phys. Rev. E **100**, 062211 (2019).
[18] I. V. Tyulkina, D. S. Goldobin, L. S. Klimenko, I. S. Poperechny, and Y. L. Raikher, Phil. Trans. R. Soc. A **378**, 20190259 (2020).
[19] T. B. Luke, E. Barreto, and P. So, Neural Comput. **25**, 3207 (2013).
[20] C. R. Laing, Phys. Rev. E **90**, 010901(R) (2014).
[21] E. Montbrió, D. Pazó, and A. Roxin, Phys. Rev. X **5**, 021028 (2015).
[22] F. Devalle, A. Roxin, and E. Montbrió, PLoS Comput. Biol. **13**, e1005881 (2017).
[23] A. Byrne, M. J. Brookes, and S. Coombes, J. Comput. Neurosci. **43**, 143 (2017).
[24] G. Dumont, G. B. Ermentrout, and B. Gutkin, Phys. Rev. E **96**, 042311 (2017).
[25] F. Devalle, E. Montbrió, and D. Pazó, Phys. Rev. E **98**, 042214 (2018).
[26] H. Schmidt, D. Avitabile, E. Montbrió, and A. Roxin, PLoS Comput. Biol. **14**, e1006430 (2018).
[27] S. Coombes and A. Byrne, in *Nonlinear Dynamics in Computational Neuroscience*, edited by F. Corinto and A. Torcini (Springer, New York, 2019), pp. 1–16.
[28] B. Pietras, F. Devalle, A. Roxin, A. Daffertshofer, and E. Montbrió, Phys. Rev. E **100**, 042412 (2019).
[29] G. Dumont and B. Gutkin, PLoS Comput. Biol. **15**, e1007019 (2019).
[30] A. Ceni, S. Olmi, A. Torcini, and D. Angulo-Garcia, Chaos **30**, 053121 (2020).
[31] M. Segneri, H. Bi, S. Olmi, and A. Torcini, Front. Comput. Neurosci. **14** (2020).
[32] H. Taher, A. Torcini, and S. Olmi, PLoS Comput. Biol. **16**, e1008533 (2020).
[33] E. Montbrió and D. Pazó, Phys. Rev. Lett. **125**, 248101 (2020).
[34] E. R. Kandel, J. H. Schwartz, T. M. Jessell, S. Siegelbaum, A. J. Hudspeth, and S. Mack, *Principles of Neural Science* (McGraw-Hill, New York, 2000), Vol. 4.
[35] C. Van Vreeswijk and H. Sompolinsky, Science **274**, 1724 (1996).

[36] J. Barral and A. D. Reyes, Nat. Neurosci. **19**, 1690 (2016).

[37] C. Geisler, N. Brunel, and X.-J. Wang, J. Neurophysiol. **94**, 4344 (2005).

[38] N. Brunel and V. Hakim, Neural Comput. **11**, 1621 (1999).

[39] N. Brunel, J. Comput. Neurosci. **8**, 183 (2000).

[40] M. Mattia and P. Del Giudice, Phys. Rev. E **66**, 051917 (2002).

[41] E. S. Schaffer, S. Ostojic, and L. F. Abbott, PLoS Comput. Biol. **9**, e1003301 (2013).

[42] T. Schwalger, M. Deger, and W. Gerstner, PLoS Comput. Biol. **13**, e1005507 (2017).

[43] B. Pietras, N. Gallice, and T. Schwalger, Phys. Rev. E **102**, 022407 (2020).

[44] M. di Volo and A. Torcini, Phys. Rev. Lett. **121**, 128301 (2018).

[45] I. Ratas and K. Pyragas, Phys. Rev. E **100**, 052211 (2019).

[46] G. B. Ermentrout and N. Kopell, SIAM J. Appl. Math. **46**, 233 (1986).

[47] See Supplemental Material, which includes Refs. [10, 21,48–50], at http://link.aps.org/supplemental/10.1103/PhysRevLett.127.038301 for a detailed derivation of the MF model [Eq. (10)] and of the expressions of $r$ and $v$ for perturbed LDs, for an estimation of the scaling of the $|W_n|$ with the noise amplitude, for the relations between conventional cumulants and pseudocumulants, for the derivation of a reference noise scale, and for a preliminary analysis of the homogenous noisy case.

[48] E. Lukacs, *Characteristic Functions* (Griffin, London, 1970).

[49] A. Pikovsky and M. Rosenblum, Phys. Rev. Lett. **101**, 264103 (2008).

[50] M. di Volo, M. Segneri, D. Goldobin, A. Politi, and A. Torcini (to be published).

[51] The Fourier transform of the Lorentzian distribution is p.v. $\int_{-\infty}^{+\infty} e^{ikV} \{a/(\pi[a^2 + (V-v)^2])\} dV = e^{ikv-a|k|}$.

[52] B. Ermentrout, Scholarpedia **2**, 1399 (2007).

[53] H. Bi, M. Segneri, M. di Volo, and A. Torcini, Phys. Rev. Research **2**, 013042 (2020).

[54] A. Renart, R. Moreno-Bote, X.-J. Wang, and N. Parga, Neural Comput. **19**, 1 (2007).

[55] H. R. Wilson and J. D. Cowan, Biophys. J. **12**, 1 (1972).

[56] I. V. Tyulkina, D. S. Goldobin, L. S. Klimenko, and A. Pikovsky, Phys. Rev. Lett. **120**, 264101 (2018).

[57] D. S. Goldobin and A. V. Dolmatova, Phys. Rev. Research **1**, 033139 (2019).

[58] I. M. Lifshitz, S. A. Gredeskul, and L. A. Pastur, *Introduction to the Theory of Disordered Systems* (Wiley, New York, 1988).